ELSEVIER

Quaternary Science Reviews 25 (2006) 455–473

QSR

Radiolaria and pollen records from 0 to 50 ka at ODP Site 1233: continental and marine climate records from the Southeast Pacific

Nicklas G. Pisias[a,*], Linda Heusser[b], Cal Heusser[c], Steven W. Hostetler[d], Alan C. Mix[a], Mysti Weber[a]

[a]*College of Oceanic and Atmospheric Sciences, Oregon State University, USA*
[b]*Lamont Doherty Earth Observatory, Columbia University, USA*
[c]*New York University, USA*
[d]*US Geological Survey, Corvallis, OR, USA*

Received 31 March 2005; accepted 30 June 2005

Abstract

Site 1233 drilled during Leg 202 of the Ocean Drilling Program provides a detailed record of marine and continental climate change in the Southeast Pacific and South American continent. Splits from over 500 samples taken at 20 cm intervals for quantitative analysis of radiolarian and pollen populations yield a temporal resolution of 200–400 years. In each sample, 39 pollen taxa and 40 radiolarian species and genera were evaluated. Age control is provided by 25 AMS ^{14}C dates [Lamy, F., Kaiser, J., Ninnemann, U., Hebbeln, D., Arz, H.W., Stoner, J., 2004. Science 304, 1959–1962]. Multivariate statistical analyses of these data allow us to conclude the following: (1) During the past 50 ka, the region of the central Chile coast is not directly influenced by polar water from the Antarctic region. (2) Changes in ocean conditions off central Chile during this time interval primarily reflect north–south shifts in the position of the South Pacific transition zone. (3) Changes in Chilean vegetation reflect comparable latitudinal shifts in precipitation and the position of the southern westerlies. (4) The first canonical variate of radiolarian and pollen records extracted from Site 1233 are remarkably similar to each other as well as to temperature records from the Antarctic, which suggests that marine and continental climate variability in the region is tightly coupled at periods longer than 3000 years. (5) The phase coupling of these climate records, which lead variations of continental erosion based on iron abundance at the same site, are consistent with a hypothesis that erosion is linked to relatively long (i.e, few thousand years) response times of the Patagonian ice sheet, and thus is not a direct indicator of regional climate.

1. Introduction

Ocean Drilling Program (ODP) Leg 202 collected a transect of drill sites in areas of high sedimentation rate along the eastern margin of the Southeast Pacific, to facilitate study of oceanographic and climatic variability on time scales of 10^2–10^3 years. Two key questions that need to be addressed to further our understanding of climate change on these time scales are: (1) what are the processes associated with climate variability and (2) how are regional-scale climate events transmitted throughout the global climate system?

Two benchmark papers on climate change in Chile provide important insights on the response of the Southeast Pacific and southern South America region to climate change during the past 50,000 years. In the first paper, Lowell et al. (1995) used an extensive set of ^{14}C dates to assess the timing of Llanquihue glacial advances of the Chilean Andes. The primary advances in the Chilean glaciers are at 13,900, 14,890, 21,000, 23,060, 26,940 and 29,360 ^{14}C years BP. Lowell et al. (1995) correlated these events to the well-known

*Corresponding author. Tel.: +1 541 737 5213; fax: +1 541 737 2064.
E-mail address: pisias@coas.oregonstate.edu (N.G. Pisias).

0277-3791/$ - see front matter © 2005 Elsevier Ltd. All rights reserved.
doi:10.1016/j.quascirev.2005.06.009

Heinrich events observed in North Atlantic sediment core V23-82 (Bond and Lotti, 1995), and inferred rapid propagation of late Pleistocene climate signals through the atmosphere and that "… the interhemispheric synchrony may indicate variations of atmospheric water vapor as the immediate source of late Pleistocene climate changes".

The second paper by Lamy et al. (2004) uses data from ODP Site 1233 to examine the oceanographic changes during the late Pleistocene. The ^{14}C-dated sea-surface temperature (SST) record, based on the alkenone index U_k^{37} at this site, is correlated to the Byrd ice core (Lamy et al., 2004). This finding suggests that the oceanographic variability of the region is of southern-hemisphere origin, reflecting changes in the position of the Antarctic Circumpolar Current (ACC). Lamy et al. (2004) note the apparent conflict in which continental records suggest global (i.e., similar to northern hemisphere) forcing of climate whereas an oceanographic record implies a link to regional (Antarctic) climate change.

Here we present two additional multivariate paleoproxy data sets from ODP Site 1233. Following the strategy of Pisias et al. (2001), we combined a study of radiolarian microfossil assemblages (a proxy for oceanographic changes) and pollen assemblages (a proxy for continental climate changes) in sample splits from ODP Site 1233. Combining these data sets with general atmospheric circulation models, we gain important new insights on climate change in the Southeast Pacific and southern South America: (1) Variations of marine plankton assemblages with affinities to regional water masses provide insights on the nature of the oceanographic circulation changes associated with SST changes estimated by geochemical methods. (2) Marine pollen records provide a proxy for regional continental climate change that complement previous estimates of continental erosion based on iron abundance (Lamy et al., 2004). (3) Statistical combination of these data sets define common modes of variability of the marine and continental systems. (4) Simulations with general atmospheric circulation models provide insights on processes of ocean variability associated with glacial boundary conditions.

2. Study site and regional setting

ODP Site 1233 was drilled in the Southeast Pacific (41.0°S, 74.45°W) in a continental margin basin at a water depth of 838 m (Mix et al., 2003). Studies from piston cores in the region show that Holocene sediments accumulated at relatively high rates (100 cm/ka) and outstanding records of marine and continental sedimentation could be extracted from these sediment cores (Lamy et al., 2001).

The large-scale oceanic circulation off Chile includes the southward-flowing Cape Horn Current, a part of the subpolar system, and the northward-flowing Peru–Chile (or Humboldt) Current, which forms the eastern boundary of the subtropical gyre of the South Pacific (Strub et al., 1998) (Fig. 1). Site 1233 lies in the transition zone between these systems, that occurs presently between 40° and 45°S and is characterized by the northernmost reaches of the southern westerly winds.

The continental climate of central Chile encompasses a transition zone between summer-dry Mediterranean climates to the north of Site 1233, and heavy year-round rainfall to the south of the site. In the southern region of the Chilean Fjords, alpine glaciation and heavy rainfall result in rapid erosion and transport of sediment from the continent to the ocean. Heavy rainfall and runoff in the south result in seasonal transport of relatively low-salinity surface waters, known as Chilean Fjord Waters, to the north (Fig. 1). Interannual variability in rainfall in this region of Chile is thought to reflect the influence of ENSO events emanating from the tropics (Dettinger et al., 2001).

2.1. Stratigraphic section, chronology and samples

At ODP Site 1233, five holes were drilled and 310 m of sediment were recovered in 46 cores at subbottom depths of 0–116 m. As is common, in multiply cored ocean drilling sites, the cores are assembled into a composite section representing, as much as possible, a continuous sampling of the sediment column. Magnetic susceptibility proved to be a very useful tool to assemble a composite section representing 136 m of continuous recovery (see Mix et al., 2003 for details). Susceptibility values ranged from 50 to over 300 units.

Twenty-five AMS ^{14}C dates on planktonic foraminifera, corrected to calendar ages (using the CALPAL correction scheme; Lamy et al., 2004), provide chronologic control for the upper 75 m of the section (0–45 ka calendar years; Fig. 2). These AMS ^{14}C ages place the Laschamp magnetic event at 42 ka, in good agreement with previous estimates (Lund et al., in press). Thus, there is very good age control for the upper 75 m. Below 85 m in the section, the appearance of an extinct radiolarian species (*Lamprocyrtus neoheteroporous*) of the early Pleistocene age suggests the possibility of reworking of sediments from 85 to about 120 m in the section. There is no evidence of reworking in sediments above 85 m. Thus, given the lack of good age control and the possibility of sediment redistribution below the interval where good AMS ^{14}C age control is available, we report here only data for the past 50,000 years.

From Site 1233, 503 samples were used for both radiolarian and pollen population analysis. Twenty cm^3 samples were taken at 20 cm intervals (equivalent to a

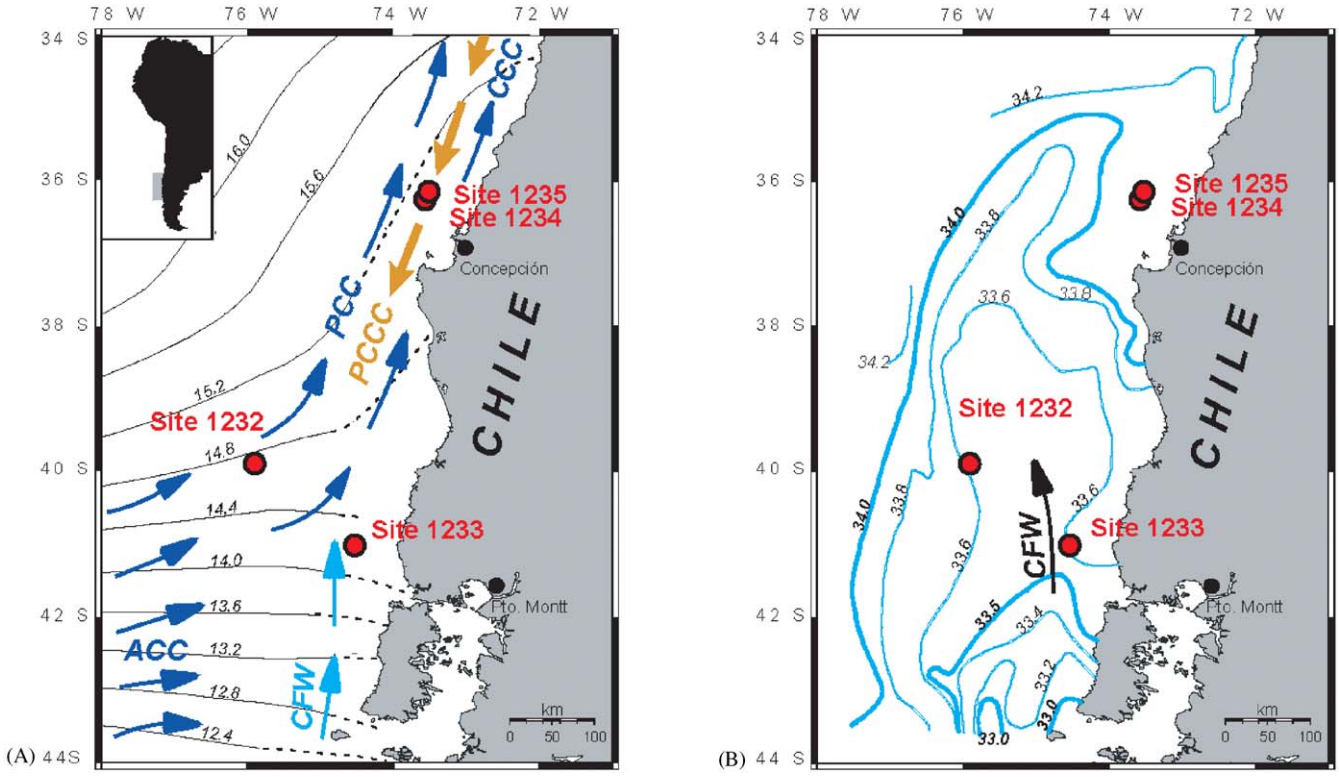

Fig. 1. (A) Sea surface temperatures in °C and surface currents of the Southeast Pacific; ACC—Antarctic Circumpolar Current; PCC—Peru Chile Current; CFW—Chilean Fijord Water; PCCC—Peru Coastal Countercurrent. (B) Surface salinity in psu. (modified from Lamy et al., 2001).

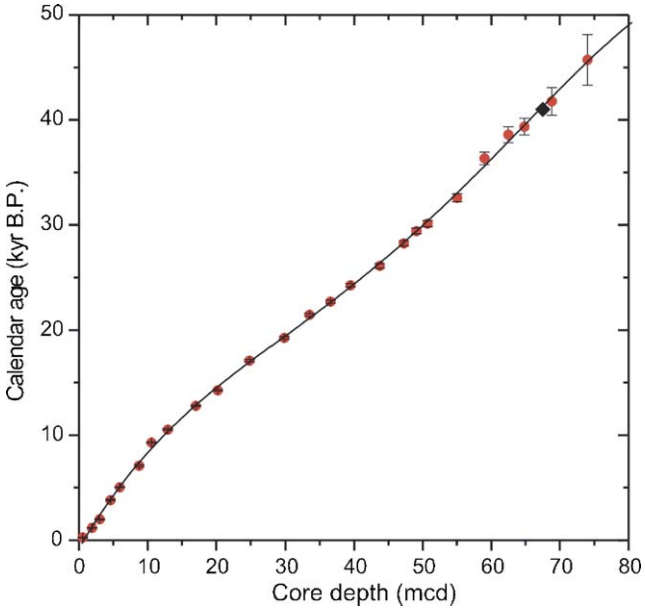

Fig. 2. Depth (in meters composite depth, mcd) versus AMS ^{14}C ages in Site 1233. From Lamy et al. (2004).

temporal spacing of 200–400 years) in a composite section. Samples were split; one split was processed for radiolarian analysis and the other was processed for pollen analysis.

3. Results and discussion

3.1. Glacial/interglacial changes in the Southeast Pacific: insights from climate models

We use climate model simulations of the Last Glacial Maximum (LGM; 21 ka calendar) to examine the plausible range of climate variability over the Southeast Pacific. We follow the strategy outlined in Pisias et al. (2001), except that here we employ an atmospheric general circulation model (GENESIS V3) to reconstruct the seasonal cycle of atmospheric circulation that is in equilibrium with specified LGM SST fields on a $2^\circ \times 2^\circ$ latitude × longitude grid rather than a regional-scale circulation model. Monthly SSTs were specified over the seasonal cycle based on the combined LGM reconstruction of CLIMAP (1981) and Mix et al. (1999), with modifications that adjust tropical and subtropical temperatures with smooth geographic pattern toward agreement with SST estimates based on geochemical proxies (Pisias et al., 2003). These adjusted LGM temperatures are considered as sensitivity tests, not a formal reconstruction. At Site 1233, they imply mean annual SSTs 4.0 °C cooler than present. For comparison, the U_k^{37} index suggests an LGM cooling of up to 5.5 °C at Site 1233 (Lamy et al., 2004). All other glacial boundary conditions, e.g., ice sheet boundaries, surface albedo, etc., are as specified in Hostetler and Mix (1999).

To assess the potential mechanisms of change in the Southeast Pacific from modern to the LGM, we used the GENESIS wind fields to calculate changes in upper-ocean transport perpendicular to the coastline and wind-stress curl over the open ocean. We compare these oceanic upwelling indices to modeled changes in precipitation and evaporation. Offshore Ekman transport was calculated along the western South America coast from 55° to 19°S (Fig. 3). Along the coast, negative values of transport are westward (offshore) and thus produce coastal upwelling, whereas positive values (onshore) produce coastal convergence or downwelling.

In the modern simulation of austral summer (Fig. 3, December), the model reproduces coastal upwelling north of 38°S and downwelling south of ~40°S. During austral winter (Fig. 3, July), coastal upwelling in the model occurs only along the coast north of 30°S. The LGM SSTs induce only small changes in modeled coastal upwelling relative to the modern simulations (Fig. 3), with a somewhat stronger coastal downwelling in winter. At the latitude of Site 1233, the model yields little or no change in coastal upwelling on an annual average basis.

In contrast to the simulations of coastal upwelling, open-ocean upwelling driven by a wind-stress curl exhibits substantial change between modern and LGM simulations. In the Peru upwelling region, a wind-stress curl supports strong upwelling (blue colors in Fig. 4). Site 1233 is located in a region where the model wind stress produces a complex pattern of change in offshore upwelling. At 41°S, the wind-stress curl is convergent in December of the modern run (Fig. 4a, red colors off the Chile coast). In July of the modern run, wind-stress curl favors upwelling off the southern Chile coast (Fig. 4c,

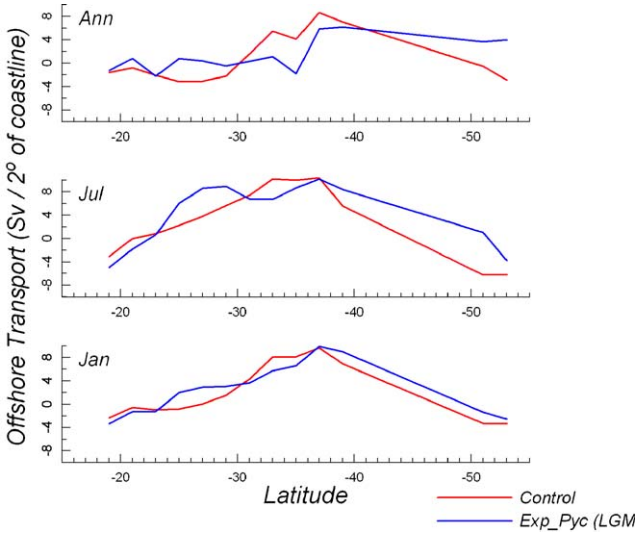

Fig. 3. Offshore Ekman transport calculated from AGCM surface winds. Transport is in Sverdrup (10^6 km^3/s) per 2° of coastline. Positive values are onshore transport, negative values offshore. Red: modern, blue: LGM.

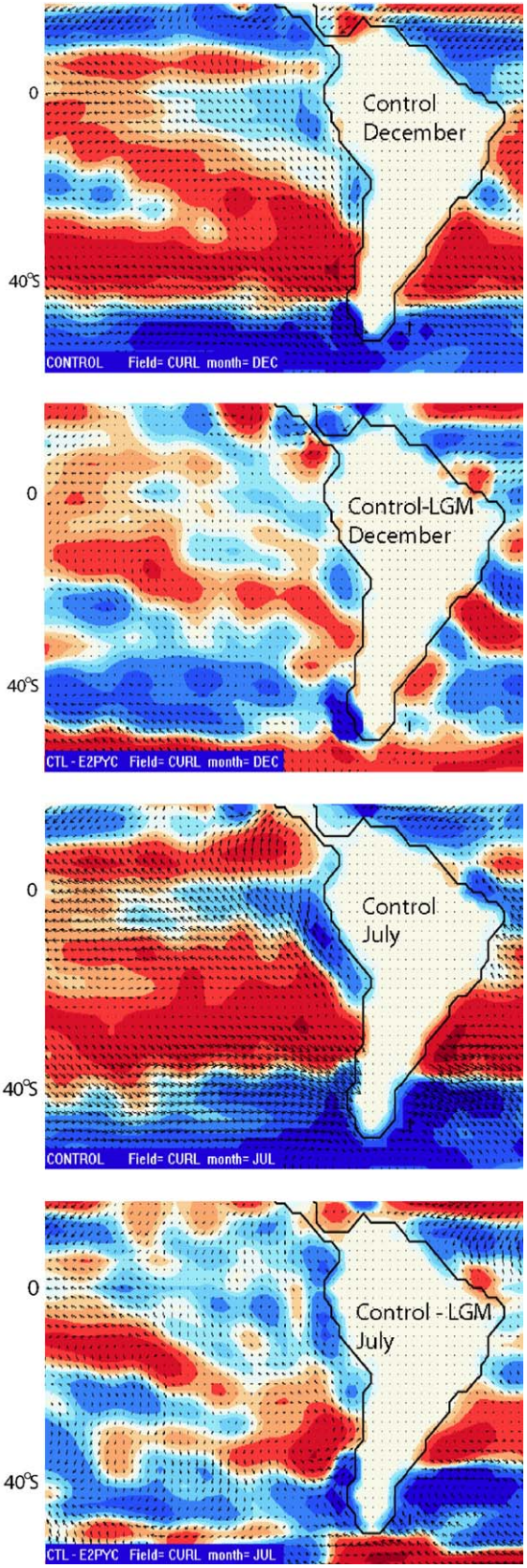

Fig. 4. Wind-stress curl calculations for December and July. Control runs and Control–LGM anomalies. Blue tones are upwelling-favorable (divergent) curl and red tones are downwelling-favorable (convergent) curl.

blue colors). In the LGM simulation, July has enhanced offshore downwelling north of Site 1233 and increased offshore upwelling to the south. In December at the Site of 1233, there is little change in the wind-stress curl relative to present (Fig. 4b, white region off the Chile coast).

The modeled glacial–interglacial response in the Southeast Pacific is different from what was calculated for similar latitudes in the Northeast Pacific (Hostetler and Bartlein, 1999; Pisias et al., 2001). Changes in the wind fields in the northern hemisphere associated with the presence of the Laurentide and Cordilleran ice sheets reduced coastal upwelling by ~50% at 40°N, whereas in the southern hemisphere we find no change at ~40°S (Fig. 3). Simulated wind-stress curl and open-ocean upwelling are similar in the two hemispheres, with greater open-ocean upwelling associated with stronger westerly winds in the latitude band 40–50° (northern hemisphere, Hostetler and Bartlein, 1999; southern hemisphere, this paper). For Site 1233, the processes of change in the model simulations predict that paleoceanographic data from the LGM should primarily reflect changes in subpolar open-ocean circulation rather than changes in coastal upwelling. This supports the conclusion of Lamy et al. (2004) that ocean condition changes would reflect changes in the position of the ACC.

3.2. Radiolaria—ocean climate record

Radiolaria microscope slides were prepared following the technique of Roelofs and Pisias (1986). Species census data were collected using the same taxonomic groups as described by Pisias et al. (1997). At least 500 specimens were counted in each sample. Pisias et al. (1997) used 170 Pacific Ocean surface sediment samples to describe the radiolarian population in terms of seven orthogonal assemblages (Pisias et al., 1997). This original data set was extended in this study to include additional 19 surface samples collected with a multicorer as part of a pre-drilling cruise survey of the Southeastern Pacific margin.

Here we use 40 radiolarian species and genera to define surface sediment assemblages (Table 1). The species groups *Tetrapyle octacantha* and *Octopyle stenozona* were not included in this analysis, because high-latitude, cold-water species can be misidentified and inadvertently grouped with warm-water *T. octacantha* and *O. stenozona* species, resulting in erroneous estimates of past conditions. A multivariate analysis of 189 surface sediment samples using a *Q*-mode factor analysis (Imbrie and Kipp, 1971; Moore, 1978; Pisias et al., 1997) identified seven radiolarian factors (Fig. 5). These groupings are very similar to those identified for Pacific sediments (Pisias et al., 1997; Moore, 1978) with the exception that with new samples from the Southeast Pacific, we identify a factor that can be associated with the Chile Current.

The first six factors using 40 species have spatial distributions essentially identical to those found in previous studies (Pisias et al., 1997) with correlation coefficients for these map distributions of 0.98, 0.99, 1.0, 0.98, 0.96 and 0.97, respectively. The first six assemblages are: (1) a subtropical (warm-water) assemblage (Fig. 5; key species: *Stylochlamydium asteriscus* and *Didymocyrtis tetrathalamus*, Tables 1 and 2); (2) an assemblage important in the transitional regions of the North and South Pacific (Fig. 6, Table 2; key species: *Botryostrobus aquilonaris*, *Lithelius minor* and *Echinomma delicatum* with a number of lesser important species, *Cycladophora bicornis, Larcopyle butschlii*, *Prunopyle antarctica*, *Pterocorys zancleus*, *P. clausus*—counted with *P. zancleus* and *Stylodictya validispin*; (3) an Antarctic assemblage (Fig. 7, Table 2; key species: *Antarctissa denticulata* and *A. strelkovi*); (4) a Bering Sea assemblage (Fig. 8, Table 2; key species: *Ceratospyris borealis*, *Cycladophora davisiana davisiana*, *C. davisiana cornutoides*); (5) an assemblage associated with the eastern boundary currents of the Pacific Basin (Fig. 9, Table 2; key species: *Pterocorys minithorax, C. davisiana davisiana*, *P. clausus* (counted with *P. zancleus*); and (6) an assemblage associated with the eastern central gyres of the Pacific in both hemispheres (Fig. 10, Table 2).

A seventh factor resolved here has a different species composition than was identified by Pisias et al. (1997), and appears to be most strongly associated with the Chile Current off the southwestern margin of South America, although it is also present in the western Pacific (Fig. 11). This assemblage accounts for a relatively small fraction of the 189 samples (reflecting the few samples from this region). The dominant species of this assemblage are *Spongopyle osculosa* and *Stylodictya validispina* (Table 1), cool-water forms that are found both in the Gulf of Alaska and in the southeastern South Pacific. An important feature of the Chile Current assemblage is the negative loading of the transitional and EBC species *P. clausus*. Thus for the Chile Current assemblage to be important, the sample must have very few *P. clausus* specimens.

To further assess possible differences in these factors from those identified by Pisias et al. (1997), a paleotemperature transfer function (not illustrated here) was generated and applied to the same data sets reported in Pisias and Mix (1997). In the 10 sediment cores used by Pisias and Mix (1997), the estimated change from modern to LGM temperatures are all within 0.5 °C of the estimates based on the Pisias et al. (1997) transfer function and the mean correlation of the 10 down-core SST time series spanning the last glacial cycle is 0.90. Thus, while the incorporation of new samples from the Southeast Pacific does not significantly change previous results from the tropics (Pisias and Mix,

Table 1
Radiolarian species and references used in this study

	Species code	Species names	Reference
1	S1	*Spongurus* sp.	p. 333, pl. 1, Fig. 2[a]
2	S1A	*Spongurus elliptica*	p. S63, pl. 8, Fig. 2[b]
3	S7	*Echinomma* cf. *leptodermum*	p. 258, pl. 3, Fig. 6[c]
4	S8	*Prunopyle antarctica*	p. S127, pl. 16, Fig. 4[b]
5	S10	*Echinomma delicatum*	p. 333, pl. 1, Fig. 5[a]
6	S12	*Euchitonia furcata* and *E. elegans*	p. S85, pl. 11, Figs. 2A and B; p. 83, pl. 11, Figs. 1A and B[b]
7	S13	*Polysolenia spinosa*	p. S19, pl. 2, Fig. 5[b]
8	S14	*Heliodiscus astericus*	p. S73, pl. 9, Figs. 1 and 2[b]
9	S17	*Hexacontium enthacanthum*	p. S45, pl. 5, Figs. 1A and B[b]
10	S18	*Hymenastrium euclidis*	p. S91, pl. 12, Fig. 3[b]
11	S23	*Didymocyrtis tetrathalamus*	p. S49, pl. 6, Fig. 1[b]
12	S24	*Lithelius minor*	p. S135, pl. 17, Figs. 3 and 4[b]
13	S29	*Larcopyle butschlii*	p. S131, pl. 17, Fig. 1[b]
14	S30	*Stylochlamydium asteriscus*	p. S113, pl. 14, Fig. 5[b]
15	S36A	*Dictyocoryne profunda*	p. S87, pl. 12, Fig. 1[b]
16	S36C	*Euchitonia triangulum*	p. 10, pl. 6, Fig. 8[d]
17	S40	*Spongaster tetras*	p. S93, pl. 13, Fig. 1[b]
18	S43	*Spongopyle osculosa*	p. 334, pl. V, Fig. 18[a]
19	S47	*Stylodictya validispina*	p. S103, pl. 13, Fig. 5[b]
20	S48	*Porodiscus* (?) sp. B	p. S109, pl. 14, Figs. 3 and 4[b]
21	N1	*Liriospyris reticulata*	p. N13, pl. 19, Fig. 4[b]
22	N2	*Anthocyrtidium ophirense*	p. N67, pl. 25, Fig. 1[b]
23	N5	*Lamprocyrtis nigriniae*	p. N81, pl. 25, Fig. 7[b]
24	N7	*Pterocorys minithorax*	p. N87, pl. 25, Fig. 10[b]
25	N9	*Giraffospyris angulata*	p. N11, pl. 19, Figs. 2A–D[b]
26	N14	*Tholospyris scaphipes*	p. N19, pl. 20, Fig. 2[b]
27	N15	*Lamprocyclas junonis*	p. 337, pl. VII, Fig. 10[a]
28	N18	*Botryostrobus auritus/australis* group	p. N101, pl. 27, Fig. 2[b]
29	N24	*Pterocanium* sp.	p. N49, pl. 23, Fig. 6[b]
30	N25/N27	*Pterocanium praetextum* and *P. eucolpum*	p. N43, pl. 23, Figs. 2 and 3[b]
31	N29	*Dictyophimus hirundo*	p. N35, pl. 22, Figs. 2–4[b]
32	N32	*Phormostichoartus corbula*	p. N103, pl. 27, Fig. 3[b]
33	N33	*Botryostrobus aquilonaris*	p. N99, pl. 27, Fig. 1[b]
34	N35	*Cycladophora davisiana davisiana*	pl. 1., Figs. 1–5[e]
35	N35A	*Cycladophora davisiana cornutoides*	pl. 1., Figs. 6–10[e]
36	N38	*Cycladophora bicornis*	pl. 15, Fig. 6[d]
37	N40	*Pterocorys clausus* and *P. zancleus*	pl. 1, Figs. 6–10 and pl. 2, Figs 10 and 11[f]
38	N42	*Theocorythium trachelium trachelium*	p. N93–N95, pl. 26, Figs. 2 and 3[b]
39	N43	*Ceratospyris borealis*	p. N9, pl. 19, Figs. 1A–D[b]
40	N48	*Antarctissa denticulata*	p. N1, pl. 18, Figs. 1A and B[b]

[a]Molina-Cruz (1977).
[b]Nigrini and Moore (1979).
[c]Robertson (1975).
[d]Moore (1974).
[e]Morley (1980).
[f]Caulet and Nigrini (1988).

1997; Pisias et al., 1997, 2002), the new samples do help to describe the radiolarian fossil populations observed at ODP Site 1233.

Samples spanning the past 50,000 years at Site 1233 can be expressed in terms of the seven modern assemblages using the methodology of Imbrie and Kipp (1971). The three most important assemblages found at Site 1233 are the transitional, the Chile Current, with the EBC assemblage (Fig. 12). There is no significant change in the abundance of cold-water fauna through the last glacial interval. The deglacial transition is, in general, marked by changes in the abundance of species associated with coastal upwelling and the transitional region (Fig. 13). These faunal changes are reflected in the increase in the Chile assemblage at the end of MIS 2.

The Antarctic assemblage, which is associated with the species group (*Antarctissa denticulata* and *A. strelkovi*), is never dominant at Site 1233 (Fig. 13). Only during short intervals in MIS 3 is this species present and then too in very low abundances (<0.5%; Fig. 13). In the modern ocean, *A. denticulata* and *A. strelkovi* are found in abundances as high as 50% in the Antarctic polar regions. Another species associated with glacial-age sediments of the Antarctic is *C. davisiana davisiana*

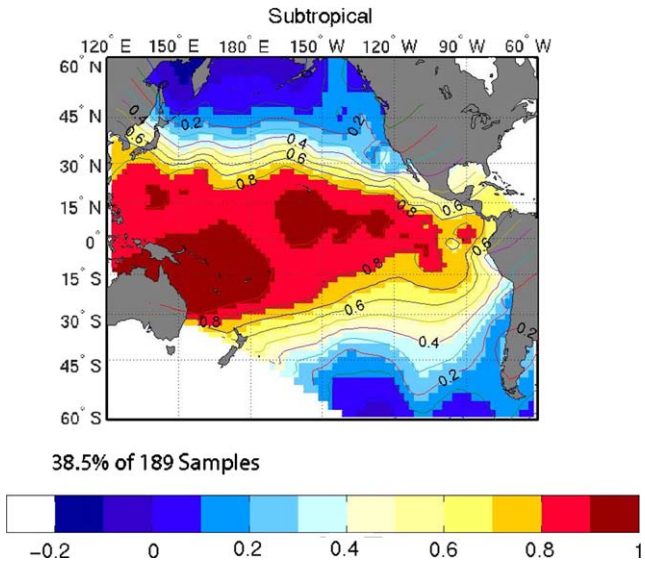

Fig. 5. Distribution of subtropical radiolarian assemblage based on a *Q*-mode factor analysis with 189 samples and 40 species.

(Fig. 13; N35). At Site 1233, this species is present only over short intervals and not at the very high abundances associated with glacial sediments in the Antarctic (abundances of this species reaches values of 45% in polar regions). It has been suggested that the water depth of Site 1233 (838 m) may effect the distribution of *C. davisiana davisiana*. In the Northeast Pacific, sites at shallower depths (F2-92-P3 799 m water depth; Sabin and Pisias, 1996) have abundances typical of the California Current region seen continuously over the same time interval spanned by Site 1233. The only site where there is evidence of a depth effect on the distribution of *C. davisiana davisiana* is in the Santa Barbara Basin where the sill depth is less than 300 m (Pisias, 1978). Thus, given the distribution of radiolarian high-latitude species, we infer that Site 1233 is not directly influenced by polar water masses from the Antarctic during the past 50 ka.

A number of species are prevalent in the assemblage associated with the transitional regions of the North and South Pacific. In general, the variability of the Transitional assemblage species is relatively similar to the species associated with the Chile Current assemblage (e.g. Fig. 13; S24, S8, S47 and S43). With two important exceptions, variations of these species prior to 20 ka appear to mimic variations in Byrd ice core $\delta^{18}O$ (using the age model of Blunier and Brook, 2001). In MIS 2, however, one species of the Transitional assemblage, *C. bicornis* (Fig. 13, N38) increases significantly in abundance (~10–12%). In surface sediments, a locus of high abundances of this species is found in the region south of Site 1233 off the coast of southernmost Chile. Surface temperatures in this region are presently 7–8 °C. Note that the down-core abundance maximum of *C. bicornis* exceeds the maximum abundance of this species in any of the surface sediment samples from the Pacific, and this implies a no-analog condition. Additionally, the species *B. aquilonaris* (Fig. 13; N33) is found in high abundances in surface sediments of the Southeast Pacific along the Chile coast just north of Site 1233. The maximum abundance of this species at Site 1233 is similar to the maximum abundances found in surface sediments.

In summary, the changes in radiolarian species abundances suggest that the oceanographic variability at Site 1233 is characterized by north–south shifts in the position at which the Antarctic Circumpolar current intersected the Chilean coast. Within the time interval we studied at Site 1233, we do not see major increases in the influence of cold waters from south of the polar front (which would be represented by the species *A. denticulata* and *A. strelkovi* or by very high abundances of *C. davisiana davisiana*).

3.3. Pollen records from Site 1233

Pollen was extracted from splits of the 503 samples used for radiolarian analyses. The relative abundance and concentration of 39 pollen and spore taxa were determined. Detailed description of these groups are presented in Heusser et al. (in press), and the pollen data are on file as a part of the ODP database.

The pollen assemblages in the sediment deposited at ODP Site 1233 derive from the vegetation biomes of Chile, which reflect latitudinal and altitudinal climatic gradients (Heusser et al., 2005; Fig. 14). Between 34° and 41°S, annual mean temperatures decrease poleward from ~15 to ~11 °C along the coast and from ~15.6 to ~14 °C (Miller, 1976; Mix et al., 2003). Offshore, the transition between surface currents at ~38°S coincides with the northernmost reaches of the southern westerlies and the major discontinuity in the annual rainfall cycle in Chile. The change from the year-round rain of southern temperate Chile to the summer-dry Mediterranean climate of northern Chile corresponds with the transition from southern temperate rainforests to northern subtropical sclerophyllous forests (Heusser, 2003). South of ~38°S, Lowland Deciduous Beech Forest occurs on lower montane slopes of the coast range and the Andes. In the central valley, this biome extends to ~41°S, where it merges with Valdivian Evergreen Forest. At ~43°S, North Patagonian and Subantarctic Evergreen Forests, floristically impoverished and structurally simpler versions of the Valdivian Evergreen Forest, develop.

Lowland Deciduous Beech Forest is composed of several *Nothofagus* species that produce *N. obliqua*-type pollen. The highly diverse arboreal component of the Valdivian Evergreen Forest includes the shade-intolerant *N. dombeyi*, opportunistic genera of the Myrtaceae and Filicinae (ferns, including *Lophosoria*

Table 2
Factor score matrix for *Q*-mode factor analysis of 40 species in 189 surface sediment samples

	Species code	Subtropical	Transitional	Antarctic	EBC	Bering Sea	Gyre	Chile current
1	S1	−0.0387	0.1376	0.1357	**0.2537**	0.0468	−0.0725	0.2141
2	S1A	0.1300	−0.0327	0.0038	−0.1188	0.0248	0.1569	0.0570
3	S7	0.0141	0.2072	0.1135	−0.0369	0.0256	−0.1108	−0.1437
4	S8	−0.0077	**0.2941**	0.0366	−0.1422	−0.0101	−0.0996	0.0338
5	S10	0.0425	**0.3236**	0.0031	0.0354	−0.0191	**0.3683**	−0.0266
6	S12	0.1973	−0.0487	−0.0355	0.1667	0.0136	0.0049	0.1677
7	S13	0.1643	−0.0065	−0.0101	−0.1255	−0.0279	0.1785	−0.0145
8	S14	0.2652	−0.0265	0.0417	−0.1339	0.0127	0.0000	−0.0093
9	S17	0.1439	0.1551	−0.0879	0.0835	−0.1140	−0.2617	0.0696
10	S18	0.1034	0.0194	−0.0161	0.1161	−0.0026	−0.0115	0.2173
11	S23	**0.4506**	−0.1209	−0.0782	**0.2868**	0.0469	0.2647	0.1091
12	S24	0.1188	**0.4216**	0.1821	−0.0106	−0.0817	**0.4518**	−0.0528
13	S29	0.0978	**0.2996**	−0.0477	−0.1087	−0.0325	−0.3886	−0.0616
14	S30	**0.6207**	−0.0098	0.0951	−0.2780	0.0710	−0.1636	−0.1106
15	S36A	0.0750	−0.0190	−0.0106	−0.0355	0.0413	−0.0183	0.1043
16	S36C	0.1415	−0.0467	−0.0230	−0.0293	0.0846	−0.0653	0.2179
17	S40	0.1943	−0.0607	−0.0189	−0.0845	0.1062	−0.1571	0.1972
18	S43	−0.0213	0.1578	0.2558	0.0435	−0.1463	−0.0206	**0.5126**
19	S47	0.0217	**0.2796**	0.1205	−0.0356	0.0591	−0.0432	**0.2961**
20	S48	0.0466	0.1103	−0.0139	0.0716	0.2614	−0.1478	−0.0169
21	N1	0.1247	−0.0466	−0.0113	0.0904	−0.0074	0.1716	−0.0171
22	N2	0.0652	−0.0210	−0.0096	0.1184	−0.0219	−0.0317	−0.0757
23	N5	−0.0063	0.0879	−0.0552	0.1889	−0.0509	0.0008	0.0234
24	N7	0.0177	−0.0546	−0.0146	**0.4789**	0.0543	−0.0078	−0.0394
25	N9	0.2175	−0.0718	−0.0145	0.0819	−0.0040	0.0151	−0.0476
26	N14	0.0697	−0.0712	0.2533	0.2113	0.0028	−0.0844	−0.0784
27	N15	0.0063	0.1792	−0.0316	0.0125	−0.1672	−0.0938	0.2568
28	N18	0.0207	0.0088	0.0004	0.2167	−0.0088	−0.0776	−0.0174
29	N24	−0.0103	0.0375	0.0037	0.0795	0.0312	−0.0289	0.0421
30	N25/N27	0.1646	−0.0251	−0.0279	0.1508	−0.0276	−0.1185	−0.0861
31	N29	−0.0016	0.1139	−0.0006	0.0164	0.0499	0.0615	−0.0503
32	N32	0.0226	−0.0162	0.0554	0.1479	0.0131	−0.0824	0.0206
33	N33	−0.0292	**0.3270**	−0.1035	−0.0275	0.1398	0.1096	−0.1532
34	N35	−0.0632	0.1115	0.1206	**0.3212**	**0.4818**	0.0225	−0.0779
35	N35A	−0.0109	0.0453	0.0281	−0.0419	**0.3365**	−0.0213	−0.0101
36	N38	0.0041	**0.2120**	−0.0378	0.0003	−0.0583	−0.0737	−0.0468
37	N40	0.1254	**0.2249**	−0.0030	**0.2381**	−0.2347	−0.2314	**−0.4508**
38	N42	0.1071	0.0014	0.0019	−0.0550	−0.0652	**0.2343**	−0.1425
39	N43	−0.0133	0.0592	−0.0682	−0.1450	**0.6228**	−0.0236	0.0016
40	N46	−0.0214	−0.1508	**0.8479**	−0.0709	0.0065	−0.0350	−0.1367

Values in bold indicate the more important species associated with each assemblage

quadripinnata). In the Rió Bueno drainage (~41°S), natural coastal vegetation is a mosaic of the more xeric *N. obliqua* forest and the more mesic *N. dombeyi* and myrtaceous forests. In North Patagonian Evergreen Forests, *N. nitida* (*N. dombeyi*-type pollen) is accompanied by the cold-resistant conifer *Podocarpus nubigena*, *Lomatia ferruginea* and the myrtaceous *Amomyrtus*. Hyperhumid Subantarctic Rainforest is dominated by cold-tolerant evergreen and/or deciduous *Nothofagus* species (all producing *N. dombeyi*-type pollen) along with the conifer *Pilgerodendron uviferum*. Both North Patagonian and Subantarctic forests grow principally on soils formed in regions that were formerly glaciated.

A clear division is seen in the sharp dichotomy in the pollen sequence from the last ~50 ka (Fig. 15). Between ~50 and ~17 ka, high-frequency oscillations and long-term trends in the dominant *N. dombeyi* record are antiphased with those of Gramineae. In MIS 3, *N. dombeyi*, as well as conifers (*Pilgerodendron* and *Podocarpus*) and ferns, display an overall upward decrease. In contrast, Gramineae increase overall to a sustained high in the younger part of MIS 3. Between ~30 and ~17 ka, low-amplitude oscillations in *N. dombeyi* contrast with high-amplitude fluctuations of Gramineae. A striking monotonic decrease in *N. dombeyi* that begins at ~17 ka and ends at ~14.5 ka coincides with a major increase in ferns, a broad peak in Myrtaceae centered at ~13–14 ka, and a short rise in Gramineae. This interval marks that start of a long-term increase in Podocarpaceae (presumably the summer-dry *P. saligna*) and ferns that continue to the present. A

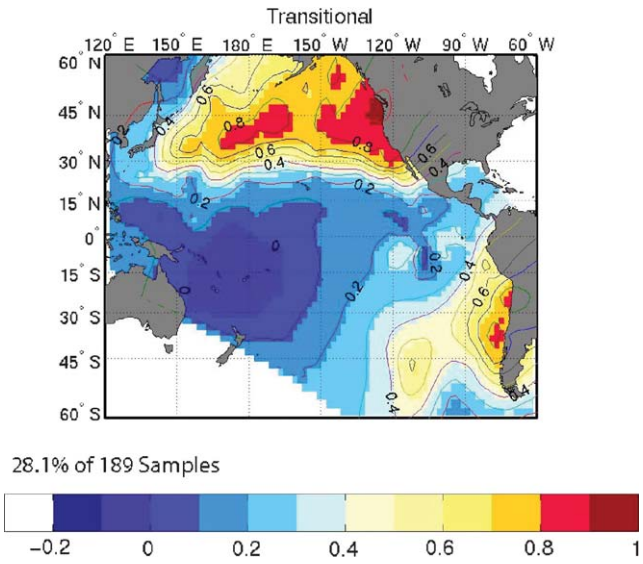

Fig. 6. Distribution of transitional radiolarian assemblage based on a *Q*-mode factor analysis with 189 samples and 40 species.

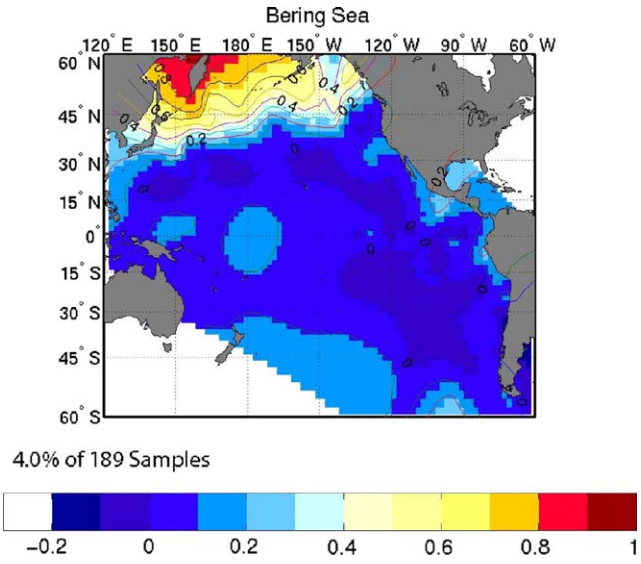

Fig. 8. Distribution of Bering Sea radiolarian assemblage based on a *Q*-mode factor analysis with 189 samples and 40 species.

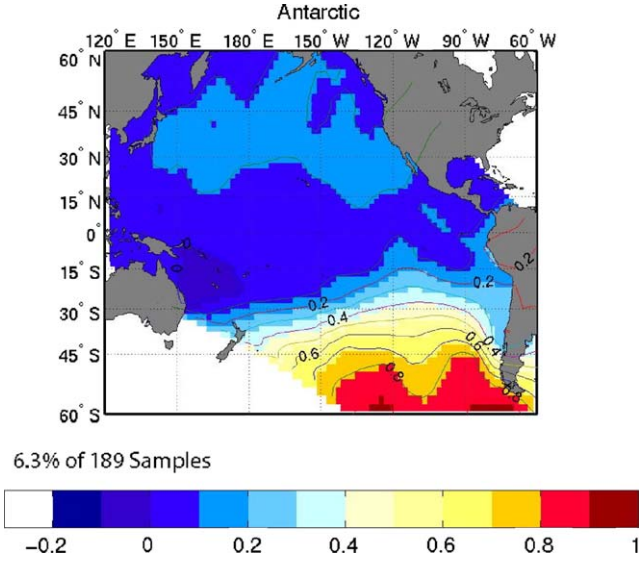

Fig. 7. Distribution of Antarctic radiolarian assemblage based on a *Q*-mode factor analysis with 189 samples and 40 species.

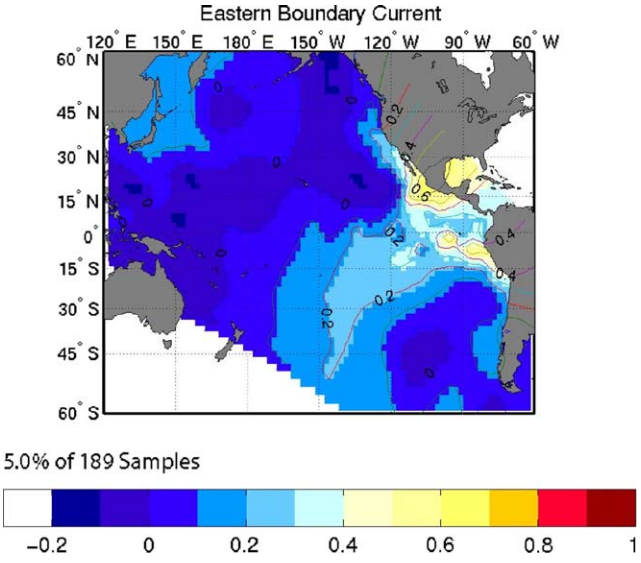

Fig. 9. Distribution of eastern boundary radiolarian assemblage based on a *Q*-mode factor analysis with 189 samples and 40 species.

minor peak in *N. dombeyi*-type occurs between ~12 and ~13 ka.

After an early Holocene rise, percentages of *N. dombeyi* remain well below glacial values and amounts of Gramineae are comparatively low. In contrast, the relative abundance of myrtaceous pollen is almost twice that of glacial values. Composite pollen, *Lomatia*, ferns and *Lophosoria* reach their highest values for the last 50 ka, while *Pilgerodendron* is essentially absent during the last ~10 ka.

During MIS 3, the pollen assemblages reflect oscillations between closed North Patagonian forests (dominated by *N. dombeyi* accompanied by *P. nubigena* and *Pilgerodendron)* and an assemblage of herbs and shrubs representative of the Subantarctic Parkland (grass-dominated park tundra which has no modern analogue). Disruption of the forests during the deglacial transition at the end of MIS-2 allows opportunistic Myrtaceae to expand. A brief re-expansion of *N. dombeyi* ~12,500–13,000 calender years BP interrupted climatic amelioration in southern Chile. MIS 1 is characterized by lowland deciduous forests and Valdivian Rain forests with ferns (including *Lophosoria*) becoming important.

Comparison of the individual pollen records with the Byrd ice core record shows, in general, good agreement with the timing of changes in the pollen record from Site 1233 and changes in temperatures over Antarctica. Specifically, the increase in abundance of Myrtaceae and

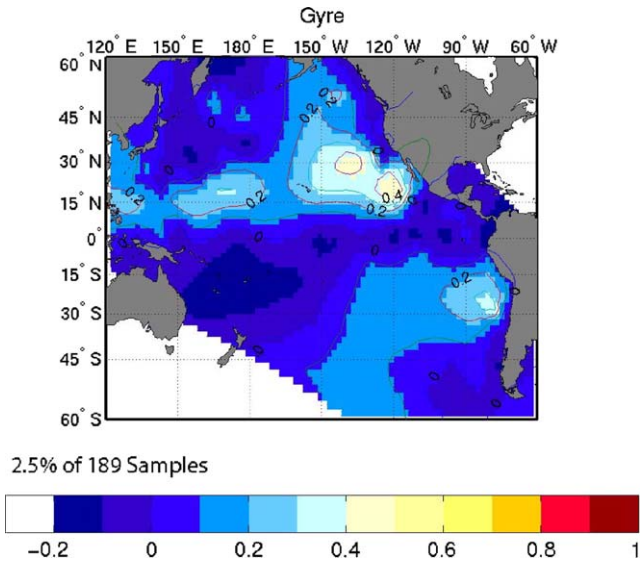

Fig. 10. Distribution of eastern central gyre radiolarian assemblage based on a *Q*-mode factor analysis with 189 samples and 40 species.

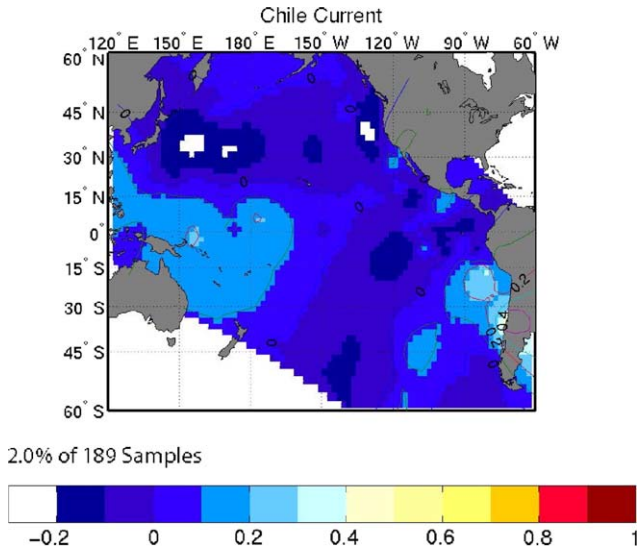

Fig. 11. Distribution of Chile radiolarian assemblage based on a *Q*-mode factor analysis with 189 samples and 40 species.

ferns (Filicinea) match very well with the increase in Antarctic temperatures at the end of the last glacial.

3.4. Chilean glacial advances and the climate records of Site 1233

Lowell et al. (1995) dated several glacial advances in the Chilean Andes and related them to North Atlantic climate events. In Figs. 12, 13 and 15 we show, as vertical lines, the times of maximum glacial advance based on the ages of Lowell et al. (1995). ^{14}C ages from Lowell et al. (1995) were corrected using CALPAL (www.calpal.de), the same calibration scheme used for the AMS ^{14}C date for Site 1233 (Lamy et al., 2004). The Lowell et al. (1995) glacial advance maxima at 13,900, 14,890, 21,000, 23,060, 26,940 and 29,360 ^{14}C years BP were thus corrected to 17,300, 18,145, 25,205, 27,900, 31,320, and 34,636 calender years.

There does not appear to be a simple relationship between oceanographic events recorded at Site 1233 and time of maximum glacial advances (Figs. 12 and 13). However, glacial advances coincide with times of increases in radiolarian species *C. bicornis* (N38, Fig. 13). In surface sediments, the maximum abundances of this species are found to the south of Site 1233 suggesting that the glacial advances are associated with a northward shift in the transition region of the Southeast Pacific. Note that glacial advances do not seem to be related changes in the presence of Antarctic species (Fig. 13).

Similar to the oceanographic record, there is no clear relationship between Chilean glacial advances and pollen records of Site 1233 (Fig. 15). However, the last glacial advance at 17,300 calender years marks the beginning of a major change in the pollen records. As noted above, this interval is marked by a marked decrease in *N. dombeyi,* which coincides with an increase in Filicinea and Myrtaceae.

3.5. Continental and marine climate linkages

Following Pisias et al. (2001), we use canonical correlation to relate oceanographic changes (as reflected in the radiolarian assemblages) to contemporaneous changes over the continent (as reflected in the pollen assemblage in the same samples). Our goal is to extract the record of climate change that is common to the eastern South Pacific Ocean and southern South America. Differences in the responses of the oceanic and continental ecosystems to climate change in this region reflect differing response times of processes associated with ocean circulation and temperature and processes of continental forest succession and ecosystems.

Canonical correlation defines the linear combination of pollen species that is most highly correlated with a linear combination of radiolarian assemblages. In using canonical correlation, we assume that some linear combination of the pollen species percentages represents a climate response. This assumption is supported by Whitlock and Bartlein (1997) who conclude that climate variations are the primary cause of regional vegetation change on millennial time scales. Likewise, we assume that a linear combination of the radiolarian assemblages reflects the oceanic response, most likely linearly related to upper ocean temperature, as is generally assumed in transfer functions (Imbrie and Kipp, 1971). However, canonical correlation differs from traditional transfer

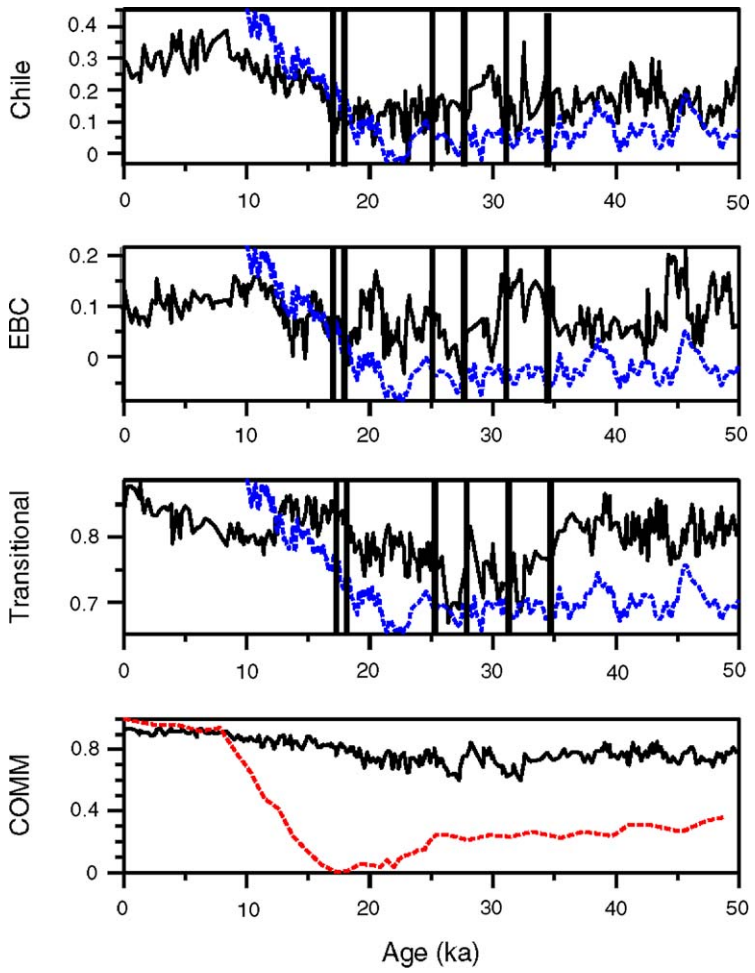

Fig. 12. Dominant radiolarian assemblages versus age in ODP Site 1233. Blue curve is the Byrd ice core $\delta^{18}O$ record for reference to a southern hemisphere climate record. Red curve is SPECMAP benthic isotope stack. COMM is factor communality showing how well down-core samples can be expressed in terms of surface sediment assemblages. Communality values can range from 0 to 1.0. Vertical lines indicate times of maximum glacial advances in Chilean Andes from Lowell et al. (1995).

function strategies. In calibrating traditional transfer functions, faunal factors are related to a single independent variable set such as SST. In contrast, canonical correlation was used here to identify the common variates between the pollen and radiolarian multivariate data sets. Twenty-four of the 40 radiolarian species were selected for canonical correlation based on their abundances in the Site 1233 samples and 14 of the 39 pollen and spore were selected based on their importance in a *Q*-mode factor analysis of the Site 1233 data set using the 39 pollen taxa. All the 22 species retained have maximum abundances in Site 1233 greater than 2.7%. The importance of each radiolarian and pollen taxa in the first canonical variate is given in Table 3. The dominate pollen taxa is Filicaeae (ferns) followed by *Lophsoria*, taxa of the fern dominate Valdivian forest–Lowland Deciduous forest while the most important radiolarian species is *Spongurus* sp, *Pterocorys minithorax* and *Lamprocyclas junonis*, species important in the eastern boundary currents of the North and South Pacific.

The canonical correlation coefficient between radiolarian and pollen variate 1 is 0.93 ($r^2 = 0.87$) and for variate 2 is 0.71 ($r^2 = 0.51$). To determine how strongly these canonical variates are related to regional climate, we compare this time series with the $\delta^{18}O$ record from the Byrd ice core (based on the age model of Blunier and Brook, 2001) (Fig. 16). The similarity in the Antarctic ice core data and the first canonical variate of radiolarians and pollen is striking. Cross-spectral analysis of these two time series using a sample interval of 200 years and over the time interval constrained by AMS ^{14}C ages shows that the coherence between the ice core $\delta^{18}O$ at frequencies lower than 0.25 cycles/ka (i.e., at periods longer than 3000 years) is significant at the 80% level and that the canonical variate 1 is in-phase with the Byrd ice core data (Fig. 17). The integrated

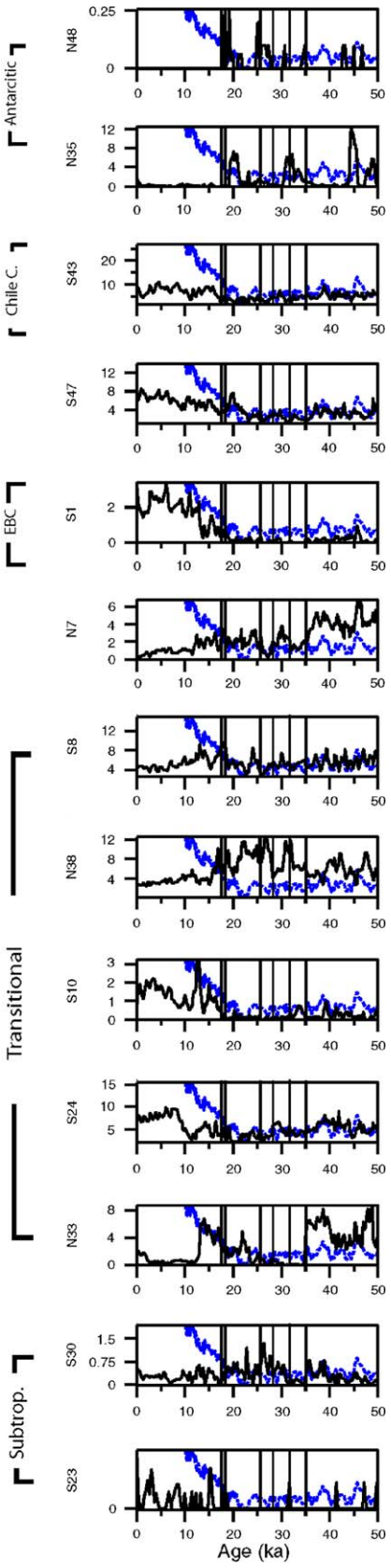

Fig. 13. Abundance of key radiolarian species of the assemblages identified in surface sediments of the Pacific. Species codes are defined in Table 1. Vertical lines indicate times of maximum glacial advances in Chilean Andes from Lowell et al. (1995).

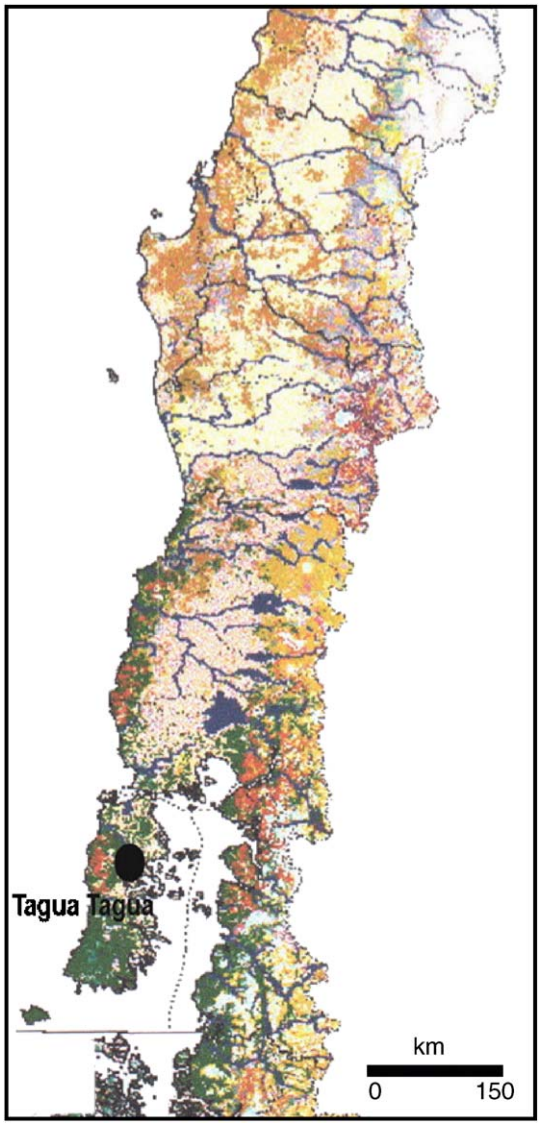

Fig. 14. Present distribution of vegetation in southern Chile. Lowland Deciduous Forest and Valdivian Evergreen Forest are in tan, North Patagonian Evergreen Forest in green, Andean Subantarctic Deciduous Beech Forest and tundra in dull red, and Andean glaciers in white. Non-forested areas are in pale yellow. The distribution of vegetation reflects latitudinal and altitudinal precipitation and temperature parameters. Annual precipitation and summer temperature range from ~800 mm and 20 °C at 34°S to ~4000 mm and 12 °C at 44°S. Precipitation increases from 1500 mm in the central depression to ~4000 mm on the crest of the cordilleras (from Heusser, 2003 and Heusser et al., 2004).

coherency between the ice core data and the first canonical variate (0.89 for the radiolarian variate and 0.85 for the pollen variate) is similar to the integrated coherency between the radiolarian and pollen variates (0.86).

The cross-spectral analysis shown in Fig. 17 spans the entire record length in common to both the Byrd $\delta^{18}O$ record and the records from Site 1233 (10–50 ka). Thus, spectra are influenced by the deglacial transition that

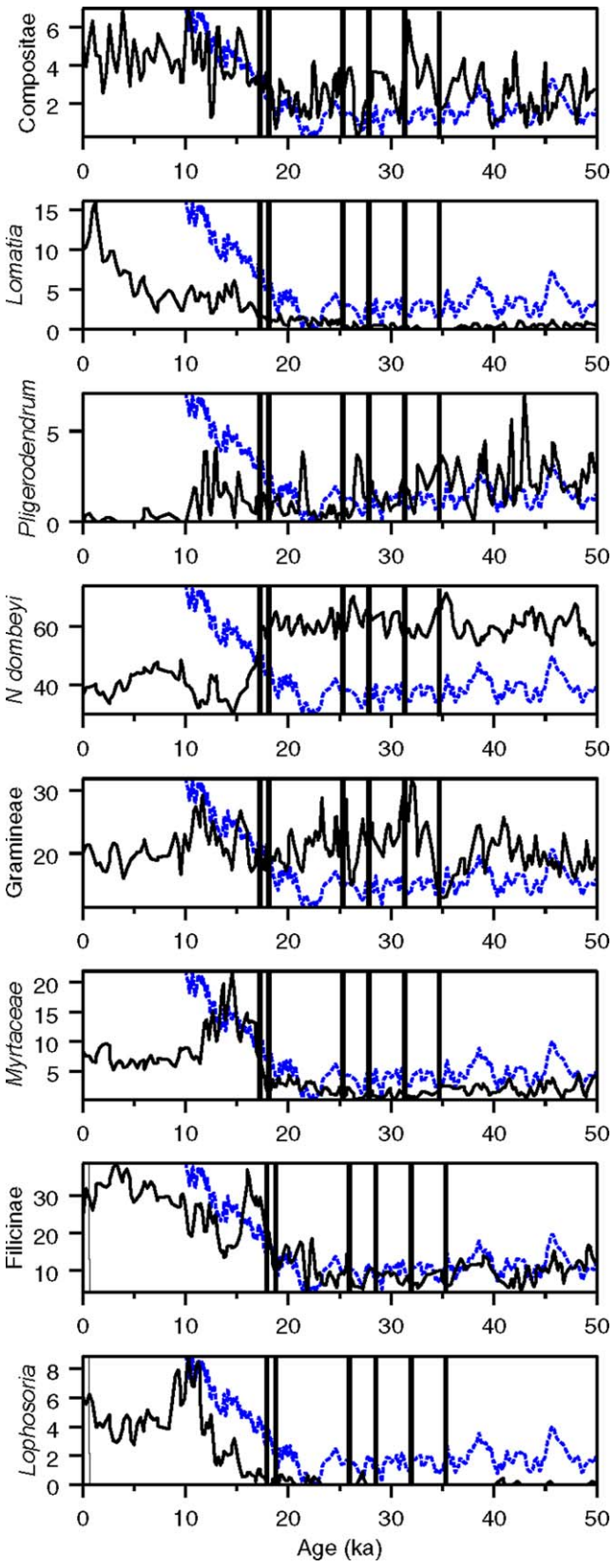

Fig. 15. Eight pollen species from Site 1233. Blue curve is the Byrd ice core $\delta^{18}O$ record for reference to a southern hemisphere climate record. Vertical lines indicate times of maximum glacial advances in Chilean Andes from Lowell et al. (1995).

Table 3
Weights for the first canonical variates comparing 24 radiolarian and 14 pollen species

Radiolaria species code[a]	Radiolaria canonical weight	Pollen canonical weight	Pollen species
S1	−0.470	0.049	*Podocarpus nubigena*
S7	0.029	−0.076	*Pilgerodendrum*
S8	−0.024	0.020	*Drimy*
S10	−0.126	−0.001	*Nothofagus obliqua*
S17	0.055	0.199	*Nothofagus dombeyi*
S18	−0.025	−0.138	*Lomatia*
S23	−0.036	−0.021	Myrtacea
S24	0.015	−0.008	*Maytenu*
S29	0.017	0.037	*Hydrangea*
S30	0.034	0.103	Tubuliferae
S43	0.011	−0.132	Composita
S47	−0.177	−0.055	Cyperaceae
S48	−0.005	−0.336	*Lophosoria*
N5	0.020	−0.519	*Filicaeae (ferns)*
N7	0.148		
N15	−0.179		
N24	−0.154		
N27	−0.017		
N29	−0.020		
N33	−0.031		
N35	0.011		
N35A	−0.018		
N40	−0.064		
N46	0.022		

[a]Species names given in Table 1.

would appear in the low-frequencies end of the spectra. To examine just the glacial interval, cross-spectral analysis was completed for the period from 20 to 50 ka (Fig. 18). In all three cross-spectra, comparing the Byrd $\delta^{18}O$ record with the pollen and radiolarian first canonical variate and the cross-spectra of the canonical variates together, there is significant coherence at low frequency as well as coherence at about 0.25 cycles/ka. At this frequency, there is again no evidence of a significant phase offset (phases between the ice core record and the canonical variates is not different from 180° and not different from 0° for the two canonical variates). Thus, while the canonical variates are calculated over the entire 0–50 ka time span of the data where the glacial transition is an important feature of the data, even within the last glacial interval the common mode of variability in the marine and continental data from Site 1233 is coherent with the Antarctic ice core record.

Canonical correlation extracts a common mode of variability in the oceanic and continental climate records that very closely matches other records of the southern hemisphere climate. This result is consistent with the conclusion of Lamy et al. (2004) that regional SSTs (based on the U_k^{37} proxy) mimic, and are in phase with climate changes recorded in Antarctica. The first canonical variate accounts for 36% of the total pollen

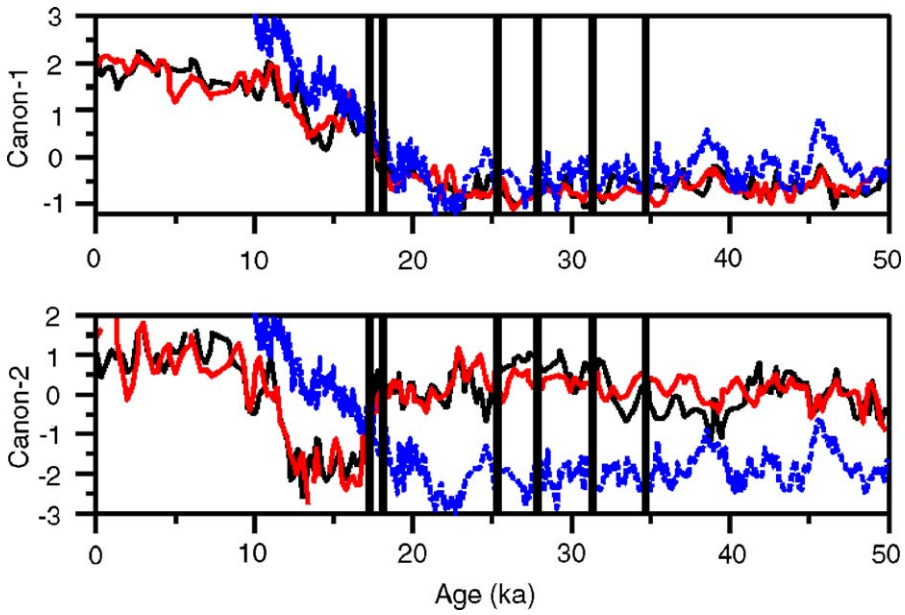

Fig. 16. The first two canonical variates from radiolarian and pollen multivariate data sets from Site 1233. Black curves are the radiolarian variates, red curves are the pollen variates and blue curves are the $\delta^{18}O$ records from the Byrd ice core (Blunier and Brook, 2001).

data and about 20% of the radiolarian data. Thus, a significant fraction of the radiolarian and pollen data are associated with other processes that are not correlated to regional climate change as represented by the Byrd ice core record. However, some of these processes may not be related to climate change but might reflect other oceanic or continental processes responsible for these paleo-records.

Lamy et al. (2004) also found that terrigenous erosion, as implied by Fe data at Site 1233, lag cold events in the same samples, might be expected given a longer response time expected for continental ice as compared to changes in ocean circulation responding to changes in atmospheric circulation. Our finding of no significant phase shift between the pollen record and the Antarctic temperature proxy suggests that the response time of the Chilean vegetation is shorter than the ice response and similar to the oceanic response. Note that canonical correlation analysis is based on linear relationships between the two multivariate data sets and the canonical variates are calculated without consideration of the time-domain nature of the data. Thus, we would not expect the radiolarian and pollen canonical variates to demonstrate any phase shifts with respect to each other. However, direct comparison of radiolarian species versus pollen species time series using cross-spectral analysis shows that, in general, phase relationships at frequencies with significant coherence tend to be either 0° or 180° and thus there is no evidence of phase shifts between these marine and continental proxies.

4. Conclusions

The paleoceanographic inferences from the Radiolaria census data from Site 1233 combined with pollen data in the same samples allow us to make the following inferences:

1. During the past 50 ka the region of the southern Chile coast is not directly influenced by polar water from the Antarctic region.
2. Changes in ocean conditions during this time interval reflect small north–south shifts in the south Pacific transition zone and its impact on the coastal waters of Chile.
3. Calculations of changes in Ekman transport expected from model-derived surface winds suggest no significant changes in coastal upwelling from modern to LGM times off the Chile coast. Radiolarian microfossil assemblage changes are consistent with the model simulations in showing little change in the coastal upwelling faunas.
4. The first canonical variate extracted from marine (radiolarian) and terrestrial (pollen species in marine sediments) climate records at Site 1233 show remarkable similarities to each other as well as to temperature records from the Antarctic. These records suggest that climate variability during the past 50 ka in the Southeast Pacific is tightly coupled at periods longer than 3000 years and not linked directly to changes in the northern hemisphere.

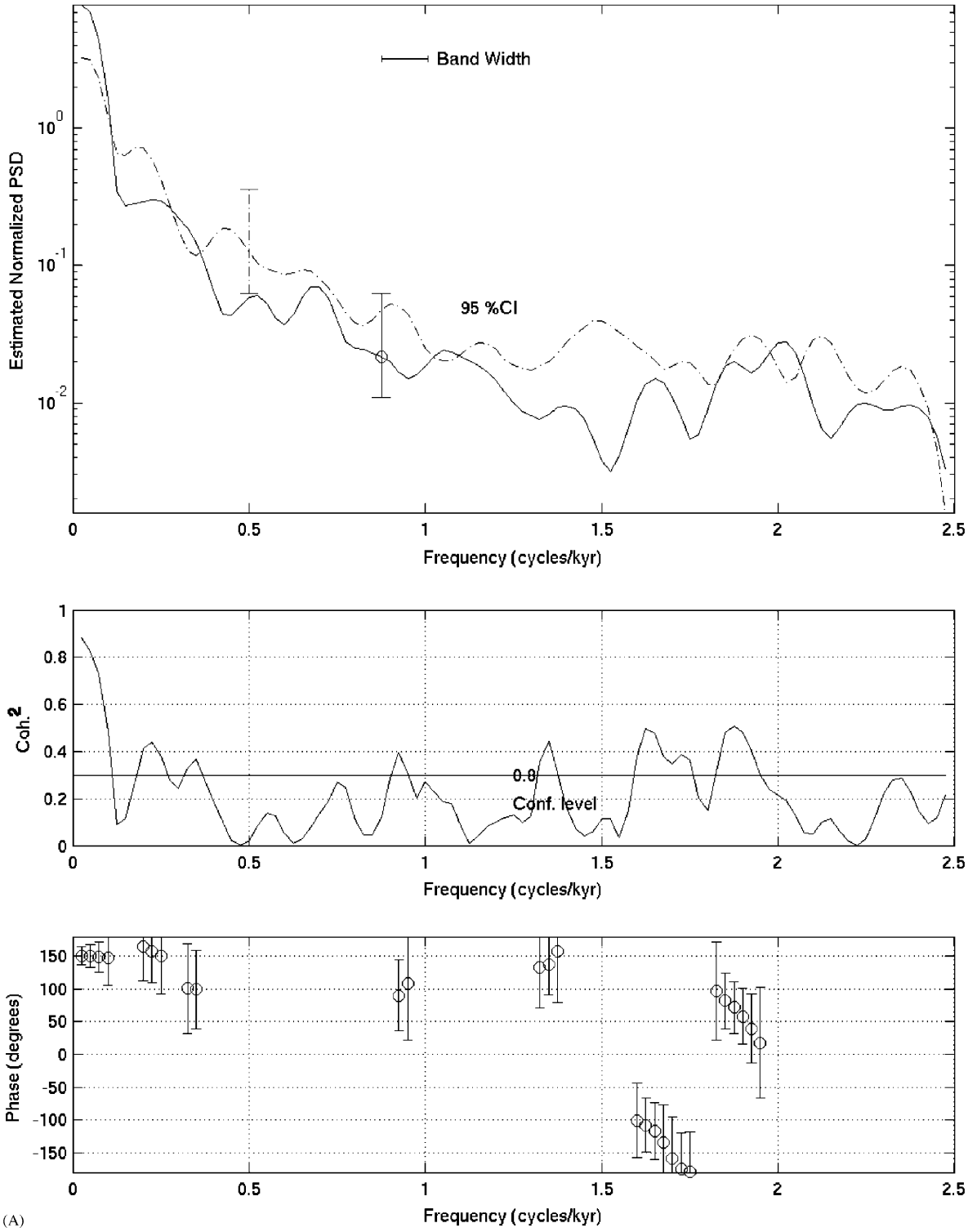

(A)

Fig. 17. Spectral calculations for 10–50 ka. (A) Cross-spectral results comparing Byrd δ^{18}O records and pollen first canonical variate. Upper frame: variance spectra of Byrd δ^{18}O records (solid) and pollen first canonical variate (dashed). Middle frame: coherence spectra with 80% confidence line for non-zero coherence. Bottom frame: phase calculations (only where coherence is non-zero at the 80% level). (B) Cross-spectral results comparing Byrd δ^{18}O records and Radiolaria first canonical variate. Upper frame: variance spectra of Byrd δ^{18}O records (solid) and radiolarian first canonical variate (dashed). Middle frame: coherence spectra with 80% confidence line for non-zero coherence. Bottom frame: phase calculations. (C) Cross-spectral results comparing pollen and Radiolaria first canonical variate. Upper frame: variance spectra of pollen (solid) and radiolarian first canonical variate (dashed). Middle frame: coherence spectra with 80% confidence line for non-zero coherence. Bottom frame: phase calculations. Calculations based on 200 data points starting at 10 ka with a $\Delta t = 200$ years and 11 degrees of freedom.

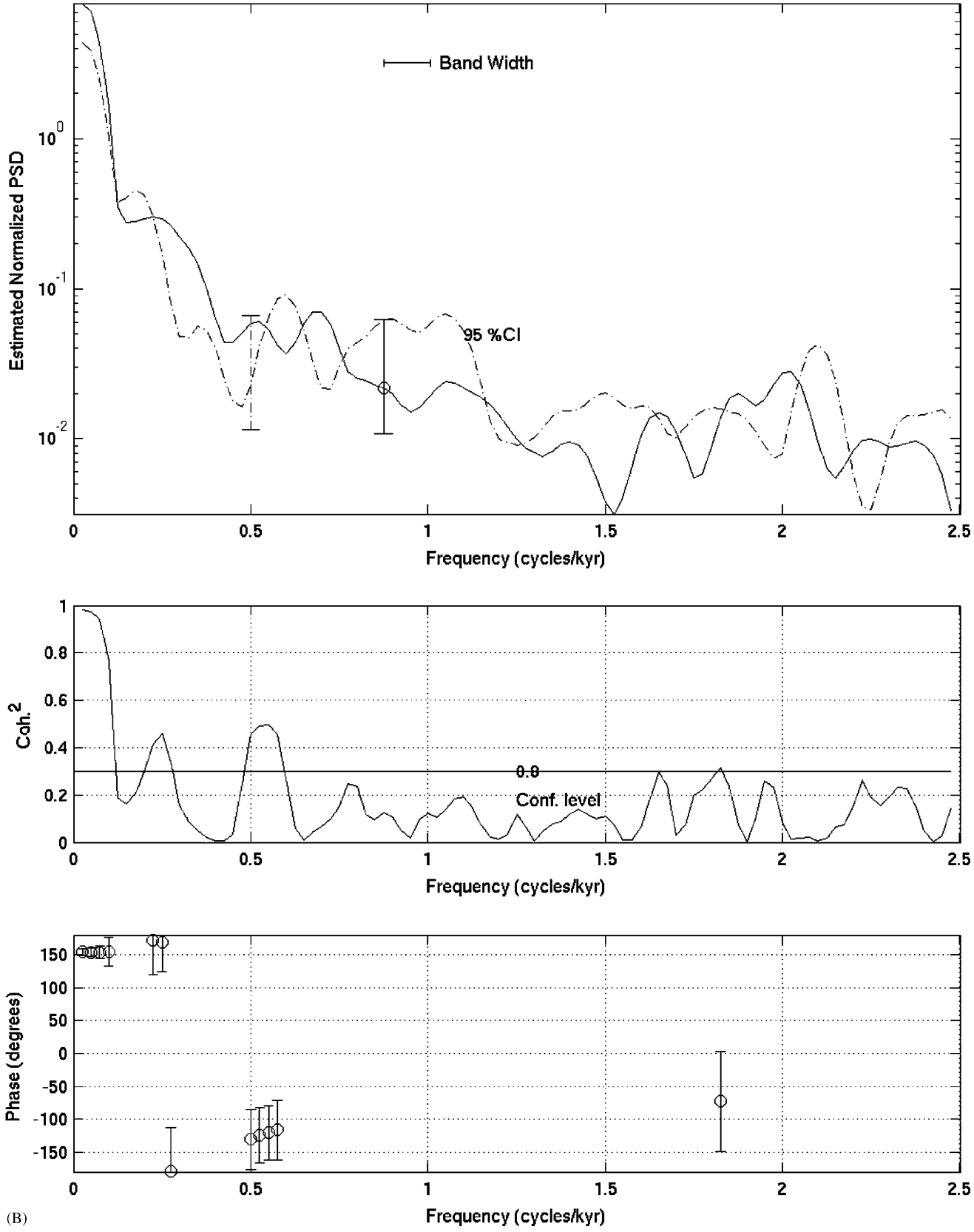

(B)

Fig. 17. (*Continued*)

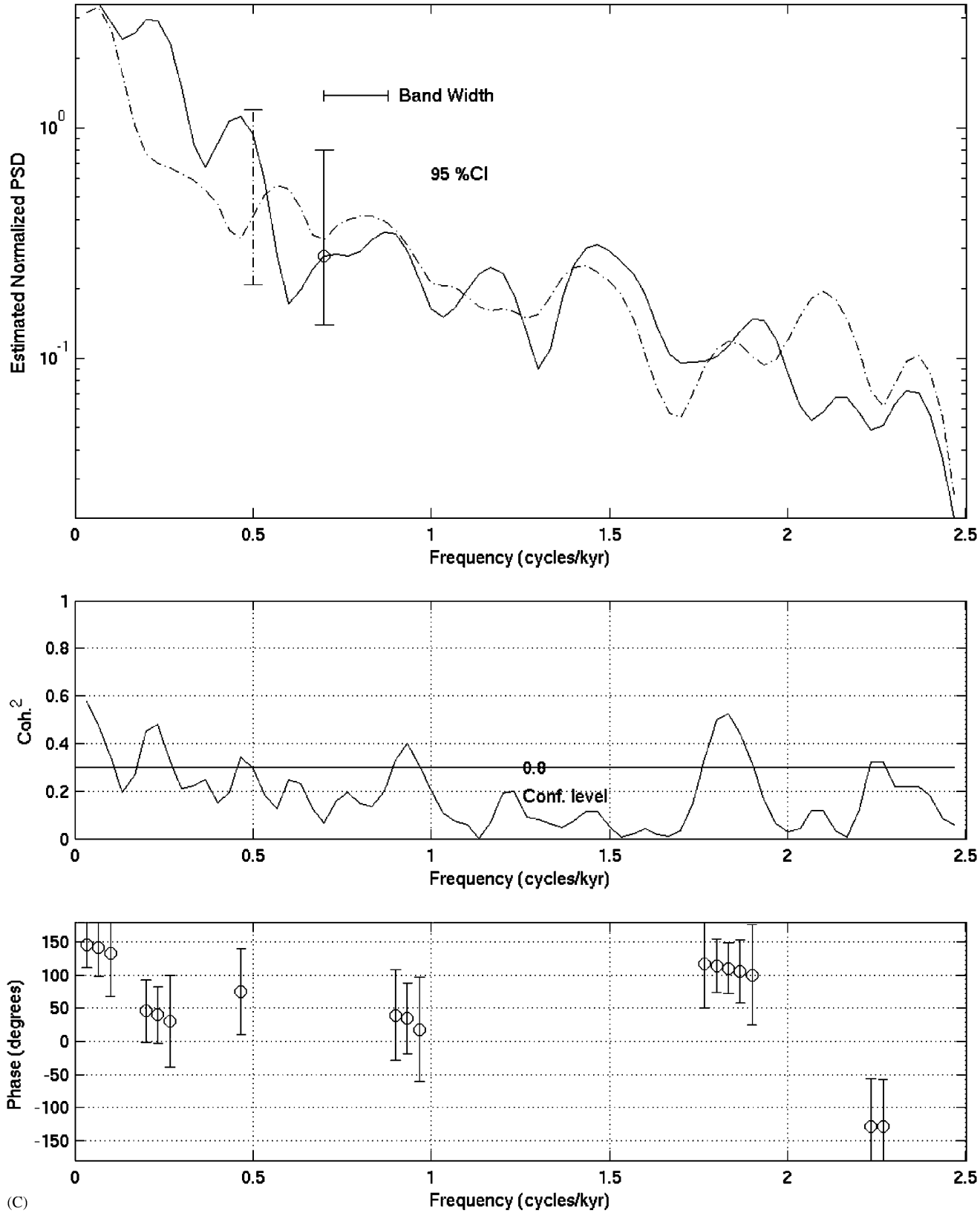

(C)

Fig. 17. (*Continued*)

5. Comparison of the Site 1233 marine- and continental-derived pollen does not show a clear relationship with respect to time of maximum Chilean glacial extent. This is likely a result of the non-continuous nature of glacial advance data.
6. The marine and terrestrial climate records from Site 1233 studied here show no phase shift in response suggesting that ocean/continental vegetation is much more tightly coupled with regional atmospheric changes (as indicated by the Antarctic isotopic temperature proxy record). This finding implies that the time lag between ocean responses and continental erosion (inferred by Lamy et al., 2004) likely reflects a long response time associated with the Patagonian ice sheet, rather than providing a direct measure of differences between continental vegetation and oceanic climate systems.
7. While there is a strong coherent response in the radiolarian and pollen data that can be related to regional climate at periods longer than 3000 years, a significant fraction of the radiolarian and pollen variability is not yet accounted for by linear relationships between data sets.

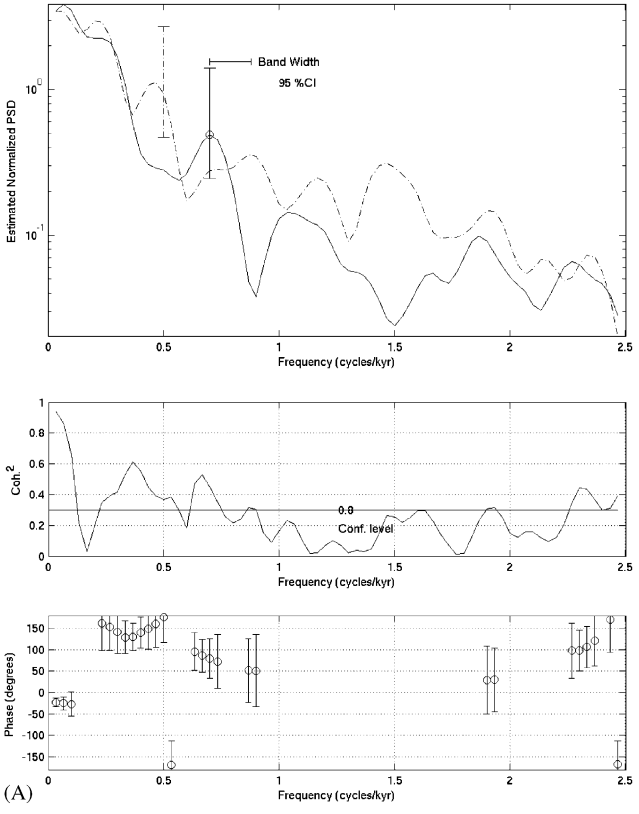

Fig. 18. Spectral calculations for 20–50 ka. Same analysis as in Fig. 17 except that calculations are based on 150 data points starting at 20 ka with a $\Delta t = 200$ years and 11 degrees of freedom. (A) Cross-spectra for Byrd δ^{18}O records and first pollen canonical variate. (B) Cross-spectra for Byrd δ^{18}O records and first radiolarian canonical variate. (C) Cross-spectral results comparing pollen and Radiolaria first canonical variate.

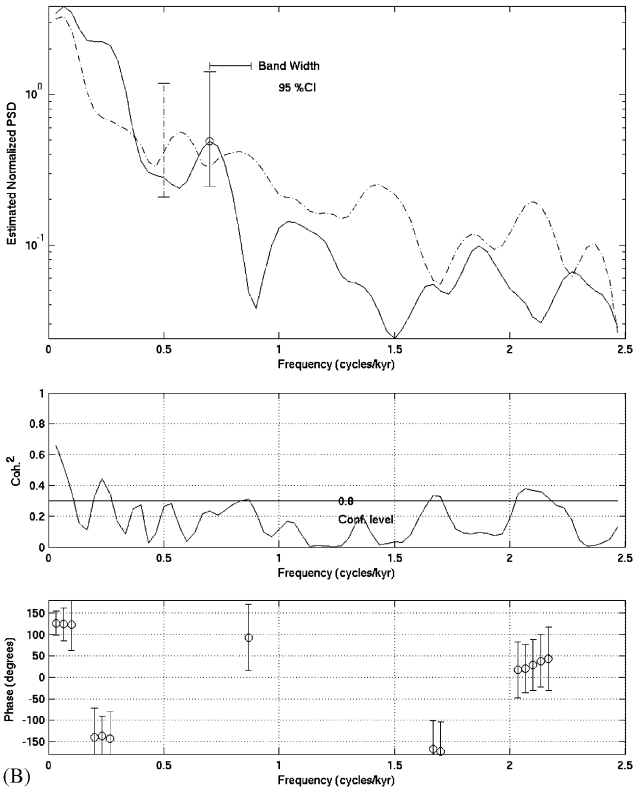

Fig. 18. (*Continued*)

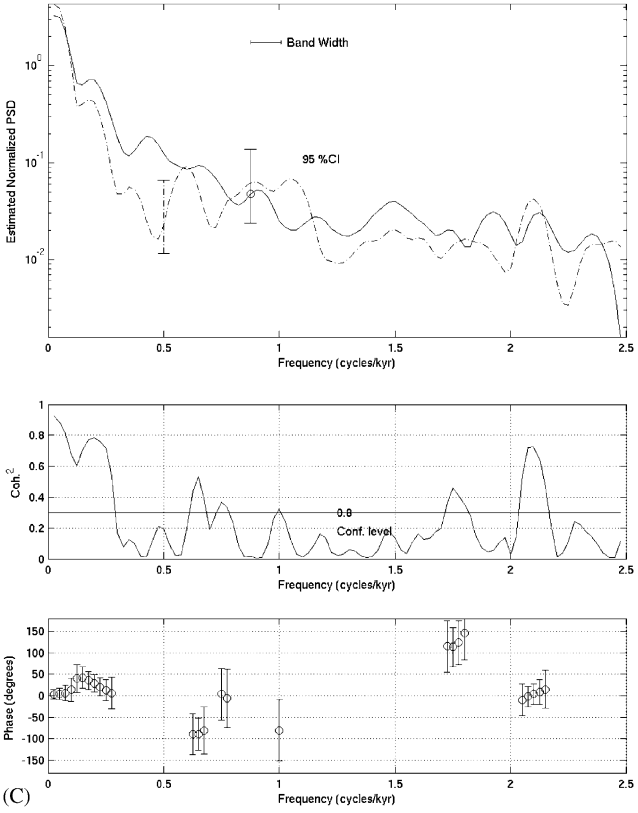

Fig. 18. (*Continued*)

Acknowledgements

This research used samples provided by the Ocean Drilling Program (ODP). ODP is sponsored by the National Science Foundation (NSF) and participating countries under management of Joint Oceanographic Institutions (JOI), Inc. We thank the Shipboard Scientific Party, Captain and crew of the *JOIDES Resolution* Leg 202. Support was provided through research grants from the National Science Foundation (ATM0135294 and ATM0319016). The manuscript was improved by reviews from Chronis Tzedakis and an anonymous reviewer.

References

Blunier, T., Brook, E.J., 2001. Timing of millennial-scale climate change in Antarctica and Greenland during the last glacial period. Science 291, 109–112.

Bond, G., Lotti, R., 1995. Science 267, 1005.

Caulet, J.P., Nigrini, C., 1988. The genus *Pterocorys* (Radiolaria) from the tropical late Neogene of the Indian and Pacific Oceans. Micropaleontology 34, 217–235.

CLIMAP (Climate: Long-Range Investigation, Mapping and Prediction Project Members), 1981. Seasonal reconstructions of the Earth's surface at the last glacial maximum. Geological Society of America Map Chart Series, MC-36.

Dettinger, M.D., Battisti, D.S., Garreaud, R.D., McCabe Jr., G.J., Blitz, C.M., 2001. Interhemispheric effects of interannual and decadal ENSO-like climate variations on the Americas. In: Markgraf, V. (Ed.), Interhemispheric Climate Linkages. Academic Press, San Diego, CA, pp. 1–16.

Heusser, C.J., 2003. Ice Age Southern Andes—A Chronicle of Palaeoecological Events. Elsevier, Amsterdam 240pp.

Heusser, L., Heusser, C., Pisias, N., 2005. Vegetation and climate dynamics of southern Chile during the past 50,000 years: results of ODP Site 1233 pollen analysis. Quaternary Science Reviews, doi:10.1016/j.quascirev.2005.04.009

Hostetler, S.W., Bartlein, P.J., 1999. Simulation of the potential responses of regional climate and surface processes in western North America to a cononical Heinrich event. In: Clark, P.U., Webb, R.S., Keigwin, L.D. (Eds.), Mechanisms of Global Climate Change at Millennial Time Scales, AGU Monograph Series, vol. 112. AGU, Washington, DC, pp. 313–327.

Hostetler, S.W., Mix, A.C., 1999. Reassessment of ice-age cooling of the tropical ocean and atmosphere. Nature 399, 673–676.

Imbrie, J., Kipp, N.G., 1971. A new micropaleontological method for quantitative paleoclimatology: application to a late Pleistocene Caribbean core. In: Turekian, K. (Ed.), Late Cenozoic Glacial Ages. Yale University Press, New Haven, CT, pp. 71–181.

Lamy, F., Hebbeln, D., Röhl, U., Wefer, G., 2001. Holocene rainfall variability in southern Chile: a marine record of latitudinal shifts of the Southern Westerlies. Earth and Planetary Science Letters 185, 369–382.

Lamy, F., Kaiser, J., Ninnemann, U., Hebbeln, D., Arz, H.W., Stoner, J., 2004. Antarctic timing of surface water changes off Chile and Patagonian ice sheet response. Science 304, 1959–1962.

Lowell, T.V., Heusser, C.J., Andersen, B.G., Moreno, P.I., Hauser, A., Heusser, L.E., Schluchter, C., Marchant, D.R., Denton, G.H., 1995. Interhemispheric correlation of late Pleistocene glacial events. Science 269, 1541–1549.

Lund, S., Stoner, J., Lamy, F., 2005. Late Quaternary paleomagnetic secular variations records and chronostratigraphy from ODF Sites 1233 and 1234. In: Mix, A., Tedeman, R., Blum, P. (Eds.), Proceedings of the Ocean Drilling Project. Scientific Results, vol. 202, in press.

Mix, A.C., Lund, D.C., Pisias, N.G., Boden, P., Bornmalm, L., Lyle, M., Pike, J., 1999. Rapid climate oscillations in the Northeast Pacific during the last deglaciation reflect northern and southern hemisphere sources. In: (Clark, P.U., Webb, R., Keigwin, L. (Eds.), Mechanisms of Global Climate Change at Millennial Time Scales, vol. 112. Geophysical Monograph, pp. 127–148.

Mix, A.C., Tiedemann, R., Blum, P., et al., 2003. Proceedings of the ODP, Initial Reports, 202: College Station TX (Ocean Drilling Program), pp. 1–145.

Molina-Cruz, A., 1977. Radiolarian assemblages and their relationship to the oceanography of the subtropical southeastern Pacific. Marine Micropaleontology 2, 315–352.

Moore Jr., T.C., 1974. Taxonomy of Holocene–Late Pleistocene Radiolaria, CLIMAP Project, unpublished.

Moore Jr., T.C., 1978. The distribution of radiolarian assemblages in the modern and ice-age Pacific. Marine Micropaleontology 3, 229–266.

Morley, J.J., 1980. Analysis of the abundance variations of the subspecies of *Cycladophora davisiana*. Marine Micropaleontology 6, 581–598.

Nigrini, C., Moore Jr., T.C., 1979. A guide to Modern Radiolaria. Foraminiferal Research 16, Cushman Foundation (special publication).

Pisias, N.G., 1978. Paleoceanography of the Santa Barbara Basin during the last 8000 years. Quaternary Research 10, 366–384.

Pisias, N.G., Mix, A.C., 1997. Spatial and temporal oceanographic variability of the Eastern Equatorial Pacific during the Late Pleistocene: evidence from Radiolaria microfossils. Paleoceanography 12 (3), 381–393.

Pisias, N.G., Roelofs, A., Weber, M., 1997. Radiolarian-based transfer function for estimating mean surface ocean temperatures and seasonal range. Paleoceanography 12 (3), 365–379.

Pisias, N.G., Mix, A.C., Heusser, L., 2001. Millenial scale climate variability of the Northeast Pacific Surface Ocean and atmosphere based on Radiolaria and pollen. Quaternary Science Reviews 20, 1561–1576.

Pisias, N.G., Hostetler, S., Mix, A., 2003. Sensitivity to uncertainties and change in the tropical and subtropical ocean during the last glacial maximum: reassessment of the CLIMAP LGM. EOS 84 (46) PP31A-03.

Robertson, J.H., 1975. Glacial to interglacial oceanographic changes in the northwest Pacific, including a continuous record of the last 400,000 years. Ph.D. Thesis, Columbia University, 251pp.

Roelofs, A.K., Pisias, N.G., 1986. Revised technique for preparing quantitative radiolarian slides from deep-sea sediments. Micropaleontology 24, 182–185.

Sabin, A., Pisias, N.G., 1996. Sea surface temperature changes in the northeastern Pacific Ocean during the past 20,000 years and their relationship to climate change in northwestern North America. Quaternary Research 46, 48–61.

Strub, P.T., Mesias, J.M., Montecino, V., Rutllant, J., Salinas, S., 1998. Coastal ocean circulation off western South America. In: Robinson, A.R., Brink, K.H. (Eds.), The Sea (Coastal Oceans), vol. 11. Wiley, New York, pp. 273–313.

Whitlock, C., Bartlein, P., 1997. Vegetation and climate change in northwest America during the past 125 kyr. Nature 388, 57–61.